RESEARCH ARTICLE

Fixed-Time Adaptive Optimal Parameter Estimation Subject to Dead-Zone and Control of Servo Systems

Shubo Wang[1] **and Xue Wang**[2,*]

[1] Faculty of Mechanical & Electrical Engineering, Kunming University of Science and Technology, Kunming 650500, China
[2] Faculty of Automation, Qingdao University, Qingdao 266071, China

Abstract

A fixed-time adaptive optimal parameter estimation (FxT-AOPE) scheme is proposed to address the difficulties in estimating dead zone parameters and slow convergence speed of tracking errors in permanent magnet synchronous motor systems. First, the continuous piecewise linear neural network is used to model the nonlinear dead zone dynamics. Second, an auxiliary filter is constructed to extract estimation errors, and this filter is used to drive an adaptive law with time-varying gain, minimizing the cost function of estimation errors and achieving adaptive optimal parameter estimation (AOPE). Then, the AOPE method is introduced into the fixed-time non-singular terminal sliding mode control (FxT-NTSMC) of the permanent magnet synchronous motor system, and the FxT-AOPE strategy is proposed to ensure the fixed time convergence of estimation error and tracking error. The stability of the closed-loop system is analyzed using Lyapunov stability theory. Finally, the feasibility of the proposed control strategy is verified through comparative simulations and experiments.

Keywords: servo system, adaptive optimal parameter estimation, fixed-time convergence, dead-zone, sliding mode control.

1 Introduction

Permanent magnet synchronous motors (PMSMs) have been more significant in various industrial applications during the past few decades [1–3]. However, non-smooth nonlinear characteristics including dead zone and friction occur during the actual production process by the mechanical connection between servo motors and mechanical devices [4]. In servo systems, the dead zone is a crucial non-smooth nonlinearity that can cause significant disruptions to system functionality or even instability [5].

Scholars have conducted extensive research to reduce the impact of nonlinear dead zones. Reference [6] used the Neural Network (NN) control method to solve the tracking problem of nonlinear systems with uncertain dead zone inputs. Reference [7] reconstructs the dead zone nonlinearity into a linear function with boundary disturbances and establishes an estimation strategy based on an observer scheme to estimate the dead zone parameters. Recently, reference [8]

Academic Editor:
Saleh Mobayen

Submitted: 05 June 2025
Accepted: 05 July 2025
Published: 28 August 2025

Vol. 2, **No.** 3, 2025.
10.62762/TSCC.2025.143677

***Corresponding author:**
✉ Xue Wang
wangxue1@qdu.edu.cn

Citation
Wang, S., & Wang, X. (2025). Fixed-Time Adaptive Optimal Parameter Estimation Subject to Dead-Zone and Control of Servo Systems. *ICCK Transactions on Sensing, Communication, and Control*, 2(3), 200–214.

proposed a sandwich system identification strategy with a dead zone, which uses CPLNN to represent the dead zone and effectively solves the problem of unmeasurable intermediate variables. However, for the above methods, they can only satisfy asymptotic convergence or exponential convergence of the control system, and their transient convergence response may be very slow.

In order to achieve faster convergence response, researchers have made various attempts at parameter estimation techniques. Reference [9] proposes an adaptive finite time parameter estimation method for nonlinear systems under persistent excitation (PE) conditions, which can directly estimate unknown time-varying parameters. The adaptive law is driven by the derived information of parameter estimation errors and has a faster convergence speed than traditional gradient descent algorithms. In reference [10], the author established a fixed time parameter estimation law for adaptive neural network control using similar concepts. However, the adaptive law proposed in the above study cannot achieve optimal convergence, that is, it cannot minimize the predetermined cost function related to estimation error.

Furthermore, from the perspective of PMSM servo system control design, SMC has been proven to be a successful method for adapting to uncertain and bounded dynamics [11]. Introducing nonlinear terms into TSMC design can achieve finite time stability [12]. However, the inherent singularity problem of TSMC can lead to a decrease in system performance and affect the control accuracy of the system. In response to this issue, experts in related fields have innovated multiple technological paths [13, 14]. However, achieving high-precision modeling and speed tracking control of PMSM systems remains a challenge. In recent years, many research results on fixed time TSMC have been widely applied in nonlinear systems.

Inspired by the above discussion, this chapter designs a fixed time adaptive optimal parameter estimation scheme for PMSM systems with dead zones, and applies it to the control system to achieve fixed time convergence of estimation error and tracking error simultaneously. Firstly, apply CPLNN to reconstruct the asymmetric dead zone model to solve the nonlinearity of the dead zone, and compensate for the dead zone based on online updated CPLNN weights. Secondly, introducing filtering operations to reduce the order of the original system and avoid the presence of acceleration variables in the regression matrix. Then, by designing auxiliary variables to construct parameter estimation errors, the cost function of estimation errors is obtained. Finally, the proposed adaptive estimation scheme will be combined with the improved FxT NTSMC method to simultaneously achieve parameter estimation and tracking control.

The main contributions of this article are summarized as follows:

1) To further improve the estimation accuracy of PMSM dead zone model parameters, an AOPE method is proposed, which includes time-varying gain in the adaptive law to improve the transient estimation response of the system.

2) Introduce the AOPE method into FxT-NTSMC to ensure that both estimation error and tracking error can achieve fixed time convergence simultaneously.

The remaining sections of this paper are organized as follows. The problem formulation is given in Section 2. Section 3 provides the Preliminaries. Section 4 describes the adaptive optimal FxT parameter estimation. The controller design and stability are shown in Section 5. Section 6 introduces the experiment verification. Finally, Section 7 draws the conclusion.

2 Problem Formulation

2.1 Dynamic Model

As Figure 1 shown, the following can describe the PMSM mathematical model.

$$\begin{cases} \dot{i}_d = -\frac{Ri_d}{L_d} + n_p\omega i_q + \frac{U_d}{L_d} \\ \dot{i}_q = -\frac{Ri_q}{L_q} - n_p\omega i_d - \frac{n_p\omega\Psi_f}{L_q} + \frac{U_q}{L_q} \\ J\dot{\omega} = \frac{3}{2}n_{_p}\Psi_f i_q - T_L - B\omega \end{cases} \tag{1}$$

where i_d and i_q denote the d-axis and q-axis stator currents; u_d and u_q represent the corresponding d-axis and q-axis stator voltages; L_d and L_q are the stator inductances along each axis, satisfying $L_d = L_q$; Ψ_f is the rotor flux linkage; n_p indicates the number of pole pairs; ω defines the angular velocity; B and J are the viscous friction coefficient and moment of inertia, respectively; T_L signifies the load torque.

To approximate the elimination of the coupling between the angular velocity and the stator current, i_d is generally designed as $i_d = 0$ to achieve approximate decoupling [15]. By selecting the state variable $x_1 = \omega$,

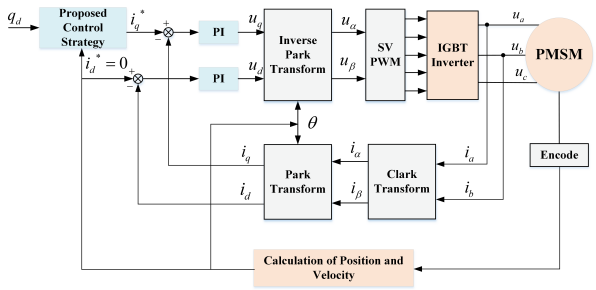

Figure 1. PMSM schematic diagram.

the system model can be expressed as:

$$\dot{\omega} = \frac{K_t i_q}{J} - \frac{B\omega}{J} + F(u) = a_0(t) + F(u) + b_0 i_q^* \quad (2)$$

where $K_t = 1.5 n_p \Psi_f$ is the torque constant. $a_0(t) = -(B\omega/J) + (K_t/J)(i_q - i_q^*) + ((K_t/J) - b_0)i_q^*$ is a measurable quantity. b_0 denotes an estimate of K_t/J , and $i_q^* = u$.

Select the state variable as $x = [x_1, x_2]^T = [\omega, a(t)]^T$, the system model can be expressed as

$$\dot{x}_1 = x_2 + F(u) + b_0 i_q^* \quad (3)$$

Assumption 1 [16]: The system states x and inputs u are both measurable and bounded.

2.2 Non-symmetric Dead-zone

Figure 2 shows a PMSM system with non-symmetric dead-zone input nonlinearity. The input $u(t)$ and unmeasurable internal signal $v(t)$ are related by the mapping $F(\cdot) : u(t) \mapsto v(t)$, which operates within the domain $U = (u_1, u_2)$ and defines the nonlinear behavior [11]. It is a piecewise linear mapping and can be precisely described by four unknown parameters l_1, D_1, l_2, D_2.

The dynamics of the asymmetric dead-zone can be illustrated as

$$v(t) = F(u(t)) = \begin{cases} l_1(u(t) - D_1), & u_1 < u(t) \le D_1 \\ 0 \quad , & D_1 \le u(t) \le D_2 \\ l_2(u(t) - D_2), & D_2 < u(t) \le u_2 \end{cases} \quad (4)$$

$$y(t) = G(v(t)) + \varepsilon(t) \quad (5)$$

where l_1 and l_2 represent the slopes of the linear area, D_1 and D_2 represent the threshold of the dead-zone area. $\varepsilon(t)$ denotes a sequence of independent and identically distributed random variables. Note that the upper and lower bounds of the dead-zone input are constrained by the given parameters u_1 and u_2.

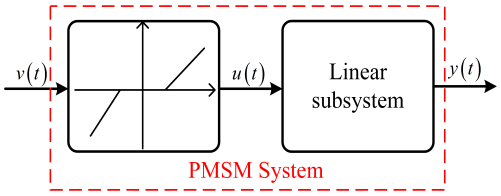

Figure 2. PMSM system with asymmetric dead-zone.

3 Preliminaries

3.1 Continuous Piecewise Linear Function

Nonlinear, nonsmooth dynamics involving dead zones cannot generally be well modeled by linear continuous functions. By leveraging the parameter-linear representation and piecewise-continuous characteristics of the CPLNN, one can construct an augmented model to approximate the dead-zone dynamics.

Definition 1 [17]: A continuous piecewise linear (CPL) function $\mathfrak{I} : S \to \mathbb{R}$ defined on a domain $S \subseteq \mathbb{R}^p$ satisfies the following necessary and sufficient conditions.

1) The domain S admits a finite partition into convex subregions $\{S_r\}_{r=1}^q$ separated by boundaries satisfying: - Each boundary is a $(p-1)$-dimensional hyperplane - No boundary lies within any $(p-2)$-dimensional hyperplane

$$\bigcup S_r = S, \mathring{S}_{r_1} \bigcap \mathring{S}_{r_2} = \phi, \forall r_1 \neq r_2, r_1, r_2 = 1, \cdots, q \quad (6)$$

For each subregion S_r, let $\mathring{S}_r$ denote its interior.

2)The CPL function $\mathfrak{I}(x)$ is expressible as a composition of q local linear functions $\aleph_r$ corresponding to $\mathring{S}_r$, with the general form:

$$\Im(x) = \max_{1 \le i \le q} \max_{r \in s_i} \aleph_r(x), \forall x \in S \quad (7)$$

where each index i, let s_i denote a nonempty subset of $\{1, 2, \ldots, q\}$.

Definition 2 [18]: Let $S \subset \mathbb{R}^p$ be compact and $\varphi : S \to \mathbb{R}$ be continuous. A continuous piecewise linear (CPL) function $\mathfrak{I} : S \to \mathbb{R}$ exists such that for any $\delta > 0$,

$$\sup_{x \in S} |\mathfrak{I}(x) - \varphi(x)| < \delta.$$

3.2 Fixed-time Stability

Consider the following time-dependent dynamic system:

$$\dot{x}(t) = f(t, x(t)), x(0) = x_0 \quad (8)$$

where $x \in \mathbb{R}^p$ denote the state, and $f : \mathbb{R}^{p+1} \to \mathbb{R}^p$ a continuous function with a unique solution. The origin is taken as the equilibrium point, i.e., $f(t,0) = 0$.

Definition 3 [18]:A system is globally fixed-time stable (FxTS) if it is globally finite-time stable (FxTS) and its settling-time function $T(x_0)$ is uniformly bounded, i.e.,

$$\exists\, T_{\max} > 0 \quad \text{such that} \quad T(x_0) < T_{\max}, \quad \forall\, x_0 \in \mathbb{R}^p.$$

Lemma 1 [19]: Suppose there exists a continuous radially unbounded function $V : \Re^n \to \Re_0^+$ for system (8) such that

1)$V(x(t)) = 0 \Leftrightarrow x(t) = 0$;

2)Any solution $x(t)$ of system () satisfies

$$\dot{V}(x) = -\gamma_1 V^{\mu_1} - \gamma_2 V^{\mu_2} \tag{9}$$

where $\gamma_1, \gamma_2 > 0$, $0 < \mu_1 > 1$, $\mu_2 > 1$.

Then, the origin of system (8) is FxTS, and the setting time $T(x_0)$ is bounded by

$$T_{\max} = \frac{\gamma_1^{\frac{1-\mu_2}{\mu_2-\mu_1}} \gamma_2^{\frac{\mu_1-1}{\mu_2-\mu_1}} \pi}{(\mu_2-\mu_1)\sin\left(\frac{1-\mu_2}{\mu_2-\mu_1}\pi\right)} \tag{10}$$

Lemma 2 [20]: If $\gamma > 1$, $z_1, z_2, \ldots, z_n \geq 0$, $0 < \beta \leq 1$, then the two following inequalities are valid.

$$\sum_{i=1}^{n} z_i^{\beta} \geq \left(\sum_{i=1}^{n} z_i\right)^{\beta} \tag{11}$$

$$\sum_{i=1}^{n} z_i^{\gamma} \geq n^{1-\gamma}\left(\sum_{i=1}^{n} z_i\right)^{\gamma} \tag{12}$$

Lemma 3 [18]: Given the specified nonlinear continuous system

$$\dot{y} = -c_1 sig^{\chi} y \tag{13}$$

where $y(0) = y_0$, $sig^{\chi} y = |y|^{\chi} sign(y)$, $\chi = \frac{m+n}{2} + \frac{m-n}{2} sign(|y|-1)$, $c_{1,2} > 0$, $m > 1$, $0 < n < 1$.

Next, the system described by the Eq. (30) converges to 0 with a fixed time, and define the maximum estimated convergence time as

$$T \leq T_{\max 1} := \frac{1}{l_1}\frac{m-n}{(m-1)(1-n)} \tag{14}$$

Lemma 4 [18]: Given the specified nonlinear continuous system

$$\dot{y} = -c_1 sig^{\gamma_1} y - c_2 sig^{\gamma_2} y \tag{15}$$

where $y(0) = y_0$, $sig^{\chi_i} y = |y|^{\chi_i} sign(y)$, $i = 1, 2$, $\chi_i = \frac{m_i+n_i}{2} + \frac{m_i-n_i}{2} sign(|y|-1)$, $m_i > 1$, $0 < n_i < 1$, $c_{1,2} > 0$.

Next, the system described by the Eq. (8) converges to 0 with a fixed time, and define the maximum estimated convergence time as

$$T \leq T_{\max 2} := \frac{2^{\frac{m-1}{2}}}{c_1^{\frac{2}{m+1}}(m-1)}\left(c_1^{\frac{2}{m+1}} + c_2^{\frac{2}{m+1}}\right)^{\frac{1-m}{2}} + \frac{1}{c_2(1-n)}\ln\left(\frac{c_1+c_2}{c_1}\right) \tag{16}$$

3.3 Excitation Condition

Definition 4 [21]: A bounded signal α satisfies the persistent excitation (PE) condition if

$$\int_{T_p-t}^{T_p} \alpha^T(s)\alpha(s)\mathrm{d}s \geq C_p I \tag{17}$$

holds for some $C_p, T_p \in \Re^+$, and all $t \in \Re_0^+$.

4 Adaptive Optimal Fxt Parameter Estimation

This section develops an innovative fixed-time optimal (FxT) adaptive scheme for system (3) to identify unknown parameters σ.

4.1 Dead-Zone Parametrization

To estimate unknown parameters in PMSM systems with dead-zone nonlinearity using exclusively input/output data, the dead-zone model requires reparameterization into an identifiable input/output structure.

By passing reliance on the unmeasurable intermediate signal $v(t)$, the dead-zone function (4) is reformulated as a continuous piecewise linear (CPL) function. Per Definition 2, a continuous piecewise linear neural network (CPLNN) models the dead-zone dynamics. Following Definition 1, the dead-zone input $u(t)$ is segmented into s non-overlapping subregions defined by boundaries α_r (lower) and β_r (upper), where each basis function $\sigma_r(\cdot)$ corresponds to the r-th subregion.

$$v(t) = F(u(t)) = \rho_0 + \sum_{r=1}^{s} \rho_r \sigma_r(0, u(t) - \alpha_r, \beta_r - \alpha_r) \tag{18}$$

where β_r denotes the upper boundary of the subregion, and α_r denotes the lower boundary of the subregion. The basis function that is utilized in the construction of the CPLNN model is $\sigma_r(0, u(t)-\alpha_r, \beta_r-\alpha_r)$, which can be described as

$$\begin{aligned} v(t) = F(u(t)) &= \sum_{r=0}^{s} \rho_r \sigma_r(0, u(t)-\alpha_r, \beta_r-\alpha_r) \\ &= \Phi\sigma\left(u(t), \alpha_r, \beta_r\right) \end{aligned} \tag{19}$$

where $\Phi = [\rho_0, \cdots, \rho_s] \in \Re^{s+1}$, $\sigma = [\sigma_0, \cdots, \sigma_s]^T \in \Re^{s+1}$, $G(\bullet)$ represents the linear transfer function in form $G(q^{-1}) = B(q^{-1})/A(q^{-1})$, the scalar polynomials $A(q^{-1})$ and $b(q^{-1})$ are represented by

$$A(q^{-1}) = 1 + a_1 q^{-1} + \cdots + a_m q^{-m} \tag{20}$$

$$B(q^{-1}) = b_1 q^{-1} + \cdots + b_n q^{-n} \tag{21}$$

Based on this, one can derive:

$$\begin{aligned} y(t) &= \sum_{i=1}^{n} b_i F(u(t)-i) - \sum_{j=1}^{m} a_j y(t-j) + \varepsilon(t) \\ &= G(\Phi_1^T \sigma_1) + \varepsilon(t) \end{aligned} \tag{22}$$

According to the characteristics of dead-zone function, the estimation of dead-zone parameters can be calculated as [19]:

$$\begin{aligned} &\hat{D}_1 = \alpha_{r1}, \hat{D}_2 = \beta_{r2}, \hat{l}_1 \\ &= \left(\sum_{r<r_1} \rho_r\right)/(r_1-1), \hat{l}_2 = \left(\sum_{r>r_2} \rho_r\right)/(s-r_2) \end{aligned} \tag{23}$$

where $r_1 = \min_{\rho_r=0} r$, $r_2 = \max_{\rho_r=0} r$.

4.2 Adaptive Parameter Estimation

For the convenience of designing the adaptive law, define $\Phi = \left[\ \Phi_1, i_q^*\ \right]$, $\sigma = [\sigma_1, b_0]^T$. Then, equation (3) can be rewritten as:

$$\dot{x}_1 = x_2 + \Phi\sigma \tag{24}$$

The filtered variables x_{1f} and Φ_f corresponding to x_1 and Φ are defined as:

$$\begin{cases} \kappa\dot{x}_{1f} + x_{1f} = x_1, x_{1f}(0) = 0 \\ \kappa\dot{\Phi}_f + \Phi_f = \Phi, \Phi_f(0) = 0 \end{cases} \tag{25}$$

The auxiliary matrix D and vector H are defined as

$$\begin{cases} \dot{D}(t) = -mD(t) + n\Phi^T(t)\Phi(t), \\ D(0) = 0 \\ \dot{H}(t) = -mH(t) + n\Phi^T(t)G^{-1}\left(y(t) - \varepsilon(t)\right), \\ H(0) = 0 \end{cases} \tag{26}$$

with $n \in \Re^+$ being a constant used to adjust the excitation level, and $m \in \Re^+$ is set to ensure the boundedness of D, H. It is noted that l plays the role of forgetting factor, which can be set as a small constant. If m is smaller, more historical information of Φ is contained in matrix H, and vice versa. Then, the solution of (26) are derived as follows:

$$\begin{cases} D(t) = n\int_0^t e^{-m(t-\tau)}\Phi^T(\tau)\Phi(\tau)\mathrm{d}\tau \\ H(t) = n\int_0^t e^{-m(t-\tau)}\Phi^T(\tau)G^{-1}\left[y(\tau) - \varepsilon(\tau)\right]\mathrm{d}\tau \end{cases} \tag{27}$$

with $D(t)$ and $H(t)$ defined in (27), we can calculate another auxiliary variable L as

$$L = H - D\hat{\sigma} \tag{28}$$

where $\hat{\sigma}$ denotes the estimation of σ. Based on (28), we can verify the following fact for the auxiliary variable L and estimation error $\tilde{\sigma} = \sigma - \hat{\sigma}$.

$$L = D\tilde{\sigma} \tag{29}$$

where, $\Upsilon = n\int_0^t e^{-m(t-\tau)}\Phi^T(\tau)\, x_2(\tau)\,\mathrm{d}\tau$ is the residual, and it satisfies $\|\Upsilon\| \le \frac{\|\Phi_f\|\,\|x_2\|}{m}$.

Remark 1: The derived variable L depends on the unknown estimation error $\tilde{\sigma}$, enabling the design of adaptive laws to acquire $\hat{\sigma}$ with guaranteed convergence. Nevertheless, constant learning gains fail to compensate for the regressor D's influence, potentially causing sluggish transient convergence. To address this limitation, we develop a novel adaptive law leveraging the extracted error L to achieve optimal parameter estimation (OPE). Specifically, a cost function incorporating L is introduced; its minimization yields a time-varying gain that enhances estimation response.

4.3 Adaptive Optimal Parameter Estimation

This section develops a novel adaptive optimal parameter estimation (AOPE) method by minimizing a cost function of the extracted error $\tilde{\sigma}$. The minimization process yields a time-varying adaptive gain that counteracts the regressor D's influence and enhances estimation performance. Leveraging [22], the cost function is defined as:

$$\begin{aligned} J(\hat{\sigma}, t) = &\frac{1}{2}\int_0^t e^{-\iota(t-\tau)} \\ &\times \frac{[H(\tau) - D(\tau)\hat{\sigma}(t)]^T[H(\tau) - D(\tau)\hat{\sigma}(t)]}{z^2(\tau)} d\tau \\ &+ \frac{1}{2}e^{-\iota t}(\hat{\sigma}(t) - \hat{\sigma}(0))^T R_0(\hat{\sigma}(t) - \hat{\sigma}(0)) \end{aligned} \tag{30}$$

where $z^2 = I + \|D^T D\|$ is utilized for the normalization of F, $R_0 = R_0^T > 0$ and $\iota > 0$ are constants. The cost function $J(\hat{\sigma}, t)$ includes the discounts of the past estimation error based on the current parameter estimate $\hat{\sigma}$ and penalties the parameter change in $[0, t]$ weighted by $e^{-\iota t} R_0$. The constant ι serves as a forgetting factor, which implies that the effect of old data and the initial error $\hat{\sigma}(0)$ are discarded exponentially as time t increases.

Unlike the cost function employed in least-squares algorithm derivation [22]—which depends on observer error—the proposed cost function $J(\hat{\sigma}, t)$ specifically incorporates the estimation error $\tilde{\sigma}$. At each time t, $J(\hat{\sigma}, t)$ exhibits strict convexity with respect to $\hat{\sigma}$, enabling parameter estimation updates that minimize the cost function to yield optimal parameter estimates (OPE). The resulting $\hat{\sigma}(t)$ satisfies:

$$\frac{\partial J(\hat{\sigma}, t)}{\partial \hat{\sigma}} = 0 \quad \forall t \geq 0$$

Given that $\frac{\partial J(\hat{\sigma},t)}{\partial \hat{\sigma}}$ represents the partial derivative of the cost function J with respect to $\hat{\sigma}$, the solution derived from (31) yields:

$$\begin{aligned}\frac{\partial J(\hat{\sigma}, t)}{\partial \hat{\sigma}} = & \int_0^t e^{-\iota(t-\tau)} \frac{-D^T(\tau)H(\tau) + D^T(\tau)D(\tau)\hat{\sigma}(t)}{z^2} d\tau \\ & + e^{-\iota t} R_0 (\hat{\sigma}(t) - \hat{\sigma}(0)) = 0\end{aligned} \tag{31}$$

Solving this equation yields:

$$\begin{aligned}\hat{\sigma}(t) = & \left(\int_0^t e^{-\iota(t-\tau)} \frac{D^T(\tau)D(\tau)}{z^2} d\tau + e^{-\iota t} R_0 \right)^{-1} \\ & \times \left(\int_0^t e^{-\iota(t-\tau)} \frac{D^T(\tau)H(\tau)}{z^2} d\tau + e^{-\iota t} R_0 \hat{\sigma}(0) \right)\end{aligned} \tag{32}$$

For the convenience of online parameter identification, based on the n non-recursive algorithms derived from equation (33), we further take the time derivative of the $\hat{\sigma}$ given in (33). For notational simplicity, define

$$\mathrm{M}(t) = \left(\int_0^t e^{-\iota(t-\tau)} \frac{D^T(\tau)D(\tau)}{z^2} d\tau + e^{-\iota t} R_0 \right)^{-1} \tag{33}$$

$$\mathrm{N}(t) = \left(\int_0^t e^{-\iota(t-\tau)} \frac{D^T(\tau)H(\tau)}{z^2} d\tau + e^{-\iota t} R_0 \hat{\sigma}(0) \right) \tag{34}$$

Then, (33) can be rewritten as $\hat{\sigma}(t) = \mathrm{M}(t)\mathrm{N}(t)$.

Considering the following matrix equality:

$$\frac{d}{dt}\mathrm{M}\mathrm{M}^{-1} = \dot{\mathrm{M}}\mathrm{M}^{-1} + \mathrm{M}\frac{d}{dt}\mathrm{M}^{-1} = 0 \tag{35}$$

The following can obtain

$$\dot{\mathrm{M}} = -\mathrm{M}\left(\frac{d}{dt}\mathrm{M}^{-1}\right)\mathrm{M} \tag{36}$$

Then, according to definition of $\mathrm{M}(t)$ as given above, the following can obtain

$$\begin{aligned}\frac{d}{dt}\mathrm{M}^{-1} &= \frac{d}{dt}\left(\int_0^t e^{-\iota(t-\tau)} \frac{D^T(\tau)D(\tau)}{z^2} d\tau + e^{-\iota t} R_0 \right) \\ &= -\iota \int_0^t e^{-\iota(t-\tau)} \frac{D^T(\tau)D(\tau)}{z^2} d\tau - \iota e^{-\iota t} R_0 \\ &\quad + \frac{D^T D}{z^2} = -\iota \mathrm{M}^{-1} + \frac{D^T D}{z^2}\end{aligned} \tag{37}$$

Substituting (38) into (37) will yield

$$\dot{\mathrm{M}} = \rho \mathrm{M} - \mathrm{M}\frac{D^T D}{z^2}\mathrm{M}, \quad \mathrm{M}^{-1}(0) = R_0 > 0 \tag{38}$$

Analogous to (38), (34) and (35) yield

$$\frac{d\mathrm{N}}{dt} = -\iota \mathrm{N} + \frac{D^T H}{z^2} \tag{39}$$

Now by differentiating (34), we can obtain the following adaptive law for online parameter estimation:

$$\dot{\hat{\sigma}} = \mathrm{M}\frac{D^T L}{z^2} \tag{40}$$

The preceding adaptive law derives from the following mathematical operations:

$$\begin{aligned}\dot{\hat{\sigma}} &= \dot{\mathrm{M}}\mathrm{N} + \mathrm{M}\dot{\mathrm{N}} \\ &= \left(\iota \mathrm{M} - \mathrm{M}\tfrac{D^T D}{z^2}\mathrm{M}\right)\mathrm{N} + \mathrm{M}(-\iota \mathrm{N} + \tfrac{D^T H}{z^2}) \\ &= \mathrm{M}\tfrac{D^T H - D^T D\hat{\sigma}}{z^2} \\ &= \mathrm{M}\tfrac{D^T L}{z^2}\end{aligned} \tag{41}$$

In the proposed adaptive law (41), the extracted estimation error $\tilde{\sigma}$ is used to drive the L-term parameter update. Consequently, the estimation-error dynamics of adaptive law (41) can be written as $\dot{\tilde{\sigma}} = -\frac{\mathrm{M}D^T D\tilde{\sigma}}{z^2}$.. Previous studies have established exponential—and in some cases finite-time—convergence properties for adaptive laws governing estimation error. Compared with those

works, the introduction of the time-varying gain M, updated via (39), eliminates the influence of the filtered regression vector D in the L-term on the transient convergence behavior of $\tilde{\sigma}$. Specifically, the gain M defined in (5-39) converges exponentially to the weighted average of $M^T M$ as characterized in (34) and (35). Moreover, since $R_0 = R_0^T > 0$ and the matrix D (defined in (26)) is positive semidefinite, M remains well-defined for all $t > 0$. Unlike classical gradient-based adaptive laws, this law is directly driven by the estimation error $\tilde{\sigma}$ and attains optimal parameter estimates by minimizing the carefully constructed cost function.

Lemma 5 [23]*:* If the regressor Φ is persistently exciting (PE), then the matrix D is positive definite; there exists a constant $\eta_1 > 0$ such that $\lambda_{\min}(D) > \eta_1 > 0$.

To establish theoretical foundations, the boundedness of M is verified preceding the presentation of key results.

Lemma 6 [23]*:* The time-varying gain M specified in (39), subject to the PE condition of Φ, implies:

$$\lambda_1 I \leq \mathrm{M}(t) \leq \lambda_2 I \tag{42}$$

where $\lambda_1 = 1/(\upsilon_{\min}(R_0) + 1/\iota)$ and $\lambda_2 = e^{\iota T} z^2/\eta_1^2$.

Proof: The solution to (38) yields:

$$\mathrm{M}^{-1}(t) = e^{-\iota t}\mathrm{M}^{-1}(0) + \int_0^t e^{-\iota(t-\tau)} \frac{D^T D}{z^2} d\tau \tag{43}$$

Considering the facts $\frac{D^T D}{z^2} \leq I$ and $\int_0^t e^{-\iota(t-\tau)} d\tau \leq 1/\iota$, we can further obtain

$$\mathrm{M}^{-1}(t) \leq \mathrm{M}^{-1}(0) + I \int_0^t e^{-\iota(t-\tau)d\tau} \leq R_0 + I/\iota \tag{44}$$

On the other hand, when the PE condition of Φ holds, the fact $\upsilon_{\min}(F) > \eta_1 > 0$ is true. Hence, one can further verify from (44) that

$$\begin{aligned} \mathrm{M}^{-1}(t) &\geq \int_0^t e^{-\iota(t-\tau)} \frac{D^T D}{z^2} d\tau \quad \geq \int_{t-T}^t e^{-\iota(t-\tau)} \frac{DF^T D}{z^2} d\tau \\ &\geq \frac{\upsilon_1^2}{z^2} e^{-\iota T} I \end{aligned} \tag{45}$$

The time-varying gain M defined by (43) exhibits boundedness for all $t > T > 0$.

Convergence properties are characterized by Theorem 1:

Theorem 1: For system (24) satisfying the PE condition, the adaptive law (41) governed by variables D, H, L in (26), (28) and gain (39) drives the estimation error $\tilde{\sigma}$ to zero exponentially.

Proof: Consider a Lyapunov function as follows:

$$V_1 = \frac{1}{2}\tilde{\sigma}^T \mathrm{M}^{-1} \tilde{\sigma} \tag{46}$$

The time derivative of V_1 is

$$\begin{aligned} \dot{V}_1 &= \tilde{\sigma}^T \Gamma^{-1} \dot{\tilde{\sigma}} + \frac{1}{2}\tilde{\sigma}^T \dot{\mathrm{M}}^{-1} \tilde{\sigma} \\ &= -\tilde{\sigma}^T \frac{D^T D}{z^2}\tilde{\sigma} + \frac{1}{2}\tilde{\sigma}^T \left(-\iota \mathrm{M}^{-1} + \frac{D^T D}{z^2}\right)\tilde{\sigma} \\ &\leq -\frac{1}{2}(\eta^2/z^2 + \iota/\lambda_2)\|\tilde{\sigma}\|^2 \\ &\leq -\mu V_1 \end{aligned} \tag{47}$$

where $\mu = \lambda_1(\eta^2/z^2 + \iota/\lambda_2)$ is a positive constant. Then, from the Lyapunov theorem, we can conclude that the estimation error $\tilde{\sigma}$ can converge to zero exponentially.

Remark 2: Lemma 5 demonstrates that the minimum eigenvalue condition $\lambda_{\min}(D) > \eta > 0$ is achievable under the conventional PE condition of Φ. This positive definiteness property will further support the convergence proof of adaptive law (41). Rather than directly validating the challenging online PE condition, Lemma 5 offers an alternative approach: verifying the excitation requirement by online computation of $\lambda_{\min}(D)$ to test $\lambda_{\min}(D) > \eta > 0$.

Remark 3: When $\rho = 0$ in (39), the gain M defined by $\frac{d}{dt}M^{-1} = \frac{D^\top D}{z^2} \geq 0$ converges to zero—a phenomenon known as gain wind-up in adaptive estimation. To resolve this issue, we introduce the forgetting factor ι, inspired by least squares algorithms, ensuring boundedness of M as established in Lemma 6.

5 Controller Design and Stability Analysis

In this section, a modified FxT-NTSMC without the singularity issue will be presented. The proposed adaptive law will be incorporated into the controller to achieve tracking control and parameter estimation simultaneously.

5.1 Fixed-time sliding-mode controller design

To construct the sliding surface, the tracking error is defined as:

$$e = x_1 - x_d \tag{48}$$

Where x_d denotes the desired angular velocity.

To enhance the anti-interference of the system, and enable the PMSM system to achieve fast and accurate

control performance. The sliding mode surface is designed as

$$s = e + \frac{1}{N(e)}\left(k_1\xi_1(e) + k_2\xi_2(e)\right) \tag{49}$$

with

$$\xi_1(e) = \begin{cases} \mathrm{sig}^{\alpha}(e), & |e| > \varepsilon \\ l_1 e + g_1 \mathrm{e}^2 \mathrm{sign}(e), & |e| \le \varepsilon \end{cases} \tag{50}$$

and

$$\xi_2(e) = \begin{cases} \mathrm{sig}^{\beta}(e), & |e| > \varepsilon \\ l_2 e + g_2 \mathrm{e}^2 \mathrm{sign}(e), & |e| \le \varepsilon \end{cases} \tag{51}$$

where $N(e) = \tau + (1-\tau)\exp(-a|e|^b)$, $0 < \tau < 1, a > 0$; b is an even integer; $\alpha = \nu_1^{sign(|e|-1)}$, $\beta = \nu_2^{sign(1-|e|)}$, $\nu_1 > 1$, $0 < \nu_2 < 1$, $k_1, k_2 > 0$, ε is a small positive constant; $l_1 = (2-k_3)\varepsilon^{k_3-1}$; $g_1 = (k_3-1)\varepsilon^{k_3-2}$; $l_2 = (2-k_4)\varepsilon^{k_4-1}$; $g_2 = (k_4-1)\varepsilon^{k_4-2}$.

Lemma 1 establishes the continuity of the sliding mode surface s and its time derivative $\dot{s}$.

$$\dot{\xi}_1(e) = \begin{cases} \alpha|e|^{\alpha-1}, & |e| > \varepsilon \\ l_1 + 2g_1|e|, & |e| \le \varepsilon \end{cases} \tag{52}$$

and

$$\dot{\xi}_2(e) = \begin{cases} \beta|e|^{\beta-1}, & |e| > \varepsilon \\ l_2 + 2g_2|e|, & |e| \le \varepsilon \end{cases} \tag{53}$$

Remark 4: Based on Lemma 1, the following equalities holds:

$$\begin{cases} \mathrm{sign}(|e|-1) = 1 & \mathrm{sign}(1-|e|) = -1, & |e| \ge 1 \\ \mathrm{sign}(|e|-1) = -1 & \mathrm{sign}(1-|e|) = 1, & |e| < 1 \end{cases} \tag{54}$$

that is

$$\begin{cases} \alpha = v_1 & \beta = \frac{1}{v_2}, & |e| \ge 1 \\ \alpha = \frac{1}{v_1} & \beta = v_2, & |e| < 1 \end{cases} \tag{55}$$

Therefore, the parameters α and β can be seen as two positive constants in the process of derivation.

Then, the derivative of s is calculated based on (7) as

$$\dot{s} = x_2 + F(u) + b_0 i_q^* - \dot{x}_d + \vartheta_1 + \vartheta_2 \tag{56}$$

with $\vartheta_1 = \frac{[k_1\dot{\xi}_1(e) + k_2\dot{\xi}_2(e)]}{N(e)}$, $\vartheta_2 = -\frac{\dot{N}(e)[k_1\xi_1(e) + k_2\xi_2(e)]}{N^2(e)}$, $\dot{N}(e) = (1-\gamma)\exp(-a|e|^b)\left(-ab|e|^{b-1}\mathrm{sign}(e)\dot{e}\right)$.

with the optical adaptive law $\dot{\hat{\sigma}}$ obtained in (41) by minimizing a cost function of the extracted error information $\tilde{\sigma}$, a further tailored FxT adaptive law for updating $\dot{\hat{\sigma}}$ is designed as

$$\dot{\hat{\sigma}} = \Gamma\left(D^T K_1 sig^{\gamma_1}(L) + D^T K_2 sig^{\gamma_2}(L)\right) + \mathrm{M}\frac{D^T L}{z^2} \tag{57}$$

where $\Gamma > 0$ is a positive constant, $K_1, K_2 > 0$, $\gamma_1 \in (0,1)$, $\gamma_2 \in (1,\infty)$.

Subsequently, an adaptive nonsingular terminal sliding mode controller is formulated:

$$u = -\frac{1}{b_0}\left[\, x_2 + \Phi^T\hat{\sigma} - \dot{x}_d + \vartheta_1 + \vartheta_2 + c_1\mathrm{sig}^{\gamma_1}s + c_2\mathrm{sig}^{\gamma_2}s \,\right] \tag{58}$$

5.2 Analysis of Stability and Convergence

Theorem 2: For the adaptive law (58) and controller (59), if the PE condition $\Phi(T_p) \le C_p I$ defined in Definition 4 is satisfied with constant $C_p, T_p \in \Re^+$, then the stability is summarized as follows

1) The estimation parameter $\hat{\theta} \to \theta$ is true with $t \to T_b$ by employing the adaptive law.

2) The system can converge from any initial position to s in a fixed time without triggering singularity problem.

Proof: First, the candidate Lyapunov function is given as

$$V = \frac{1}{2}s^2 + \frac{1}{2}\tilde{\sigma}^T\Gamma^{-1}\tilde{\sigma} \tag{59}$$

Based on the *Lemma 3* and the system (3), differentiating V yields

$$\begin{aligned} \dot{\mathrm{V}} &= s\dot{s} + \tilde{\sigma}^T\Gamma^{-1}\dot{\tilde{\sigma}} \\ &= s\left(x_2 + F(u) + b_0 i_q^* - \dot{x}_d + \vartheta_1 + \vartheta_2\right) - \tilde{\sigma}^T\Gamma^{-1}\dot{\hat{\sigma}} \\ &= s\left(\Phi^T\tilde{\sigma} - c_1\mathrm{sig}^{\gamma_1}s - c_2\mathrm{sig}^{\gamma_2}s\right) - \tilde{\sigma}^T[\Phi^T s \\ &\quad + D^T K_1\mathrm{sig}^{\gamma_1}(L) + D^T K_2\mathrm{sig}^{\gamma_2}(L) + \Gamma^{-1}\mathrm{M}\tfrac{D^T L}{z^2}] \\ &\le -c_1\mathrm{sig}^{\gamma_1}s - c_2\mathrm{sig}^{\gamma_2}s - D^T K_1\mathrm{sig}^{\gamma_1}(L)\tilde{\sigma}^T \\ &\quad - D^T K_2\mathrm{sig}^{\gamma_2}(L)\tilde{\sigma}^T \end{aligned} \tag{60}$$

Then we have

$$\begin{aligned} &-D^T K_1\mathrm{sig}^{\gamma_1}(L)\tilde{\theta}^T - D^T K_2\mathrm{sig}^{\gamma_2}(L)\tilde{\theta}^T \\ &= -K_1 L^T\mathrm{sig}^{\gamma_1}(L) - K_2 L^T\mathrm{sig}^{\gamma_2}(L) \\ &-K_1\Upsilon^T\mathrm{sig}^{\gamma_1}(L) - K_2\Upsilon^T\mathrm{sig}^{\gamma_2}(L) \end{aligned} \tag{61}$$

Based on (62), we rewrite the equality (61) as

$$\dot{V} \le -c_1 sig^{\gamma_1}s - c_2 sig^{\gamma_2}s + K_1 L^T sig^{\gamma_1}(L) + K_2 L^T sig^{\gamma_2}(L) \tag{62}$$

Due to the Lemma 1, we can get

$$\dot{V} \leq -c_1(s^2)^{\frac{1+\gamma_1}{2}} - c_2(s^2)^{\frac{1+\gamma_2}{2}} - \mathrm{K}_1(L^TL)^{\frac{1+\gamma_1}{2}} - \mathrm{K}_2(L^TL)^{\frac{1+\gamma_2}{2}} \tag{63}$$

Then, we consider the control problem on $t \in [T_P, \infty]$. By submitting (29) into the last two terms of (64), the following inequality is proposed

$$-\mathrm{K}_1(L^TL)^{\frac{1+\gamma_1}{2}} - \mathrm{K}_2(L^TL)^{\frac{1+\gamma_2}{2}} \leq -\mathbb{K}_1(\tilde{\theta}^T\tilde{\theta})^{\frac{1+\gamma_1}{2}} - \mathbb{K}_2(\tilde{\theta}^T\tilde{\theta})^{\frac{1+\gamma_2}{2}} \tag{64}$$

where $\mathbb{K}_1 = \mathrm{K}_1 \cdot \eta^{1+\gamma_1}$, $\mathbb{K}_2 = \mathrm{K}_2 \cdot \eta^{1+\gamma_1}$.Considering the Lemma 1 and submitting (65) into (64), we finally obtain

$$\dot{V} \leq -\hbar_1 V^{\frac{1+\gamma_1}{2}} - \hbar_2 V^{\frac{1+\gamma_2}{2}} \tag{65}$$

with $\hbar_1 = 2^{\frac{1+\gamma_1}{2}} \min\left\{c_1/\lambda_{\max}^{\frac{1+\gamma_1}{2}}(L), \mathrm{K}_1/\lambda_{\max}^{\frac{1+\gamma_1}{2}}(\Gamma^{-1})\right\}$;
$\hbar_2 = 2^{\frac{1+\gamma_1}{2}} \min\left\{c_2/\lambda_{\max}^{\frac{1+\gamma_1}{2}}(L), \mathrm{K}_2/\lambda_{\max}^{\frac{1+\gamma_1}{2}}(\Gamma^{-1})\right\}$.
According to the Definition 1 and Lemma 1, the sliding mode variable and estimation error can achieve convergence in T, where $T = T_b + T_p$, and T_b can be calculated from the above inequality as follows

$$T_b = \frac{2}{\hbar_1(1-\gamma_1)} + \frac{2}{\hbar_2(\gamma_2 - 1)} \tag{66}$$

6 Simulation and Experimental Verification

The dead-zone model can be described by the following expression:

$$v(t) = F(u(t)) = \begin{cases} l_1(u(t) - D_1), & D_1 < u(t) \leq u_2 \\ 0 \quad , & -D_2 \leq u(t) \leq D_1 \\ l_2(u(t) + D_2), & u_1 \leq u(t) < -D_2 \end{cases} \tag{67}$$

In both the simulation and experimental processes, the dead-zone input range $[u_1, u_2] = [-9, 9]$ is divided into 20 segments, with the partition points given as: (-9, -7.757, -6.514, -5.271, -4.029, -2.786, -1.543, -0.3, 0.204, -0.108, 0.012, 0.084, 0.18, 1.282, 2.385, 3.487, 4.59, 5.692, 6.795, 7.897, 9).

To evaluate the control and parameter estimation performance of the system, a comparative analysis is conducted under the target speed $s_1 = 1000$ r/min, between the proposed parameter estimation–based improved fixed-time nonsingular terminal sliding mode controller (PE-FxT-NTSMC), the conventional PI control method, and the fixed-time nonsingular terminal sliding mode controller (FxT-NTSMC). Considering the viscous friction and high-frequency disturbances in the permanent magnet synchronous motor (PMSM), the load torque is configured as follows:

$$T_L = \begin{cases} 0\,N \cdot m, & 0 \leq t < 5s \\ 3\,N \cdot m, & 5 \leq t < 10s \\ 0\,N \cdot m, & 10 \leq t < 14s \end{cases} \tag{68}$$

To further verify the accuracy of the proposed control method, the target speed is set as follows:

$$s_2 = \begin{cases} 400\,r/\min, & 0 \leq t < 5s \\ 800\,r/\min, & 5 \leq t < 10s \end{cases} \tag{69}$$

In engineering applications, it is essential to provide guidelines for selecting the parameters of the proposed control algorithm. The parameters are categorized into two groups: 1) Controller parameters: k_1, k_2, c_1, and c_2; 2) Fixed-time optimal adaptive law parameters for the parameter estimation scheme: κ_1, κ_2, γ_1, γ_2, and Γ. Based on this, the parameter tuning guidelines are as follows:

1) Selecting appropriate controller parameters k_1, k_2, c_1, and c_2 can enhance the tracking performance of the system. Increasing the values of k_1 and k_2 can accelerate the response during the startup phase; however, excessively large values may increase the system's computational burden and lead to larger overshoots at the initial stage of the dynamic response. Larger values of c_1 and c_2 can shorten the convergence time and improve the convergence rate, but may also intensify chattering to some extent.

2) The adaptive law parameters κ_1, κ_2, γ_1, γ_2, and Γ should not be set too large. Their values should be chosen with a balanced consideration of parameter estimation speed and accuracy, and should be tuned reasonably during actual system operation and adjustment.

6.1 Simulation verification

The key parameter configuration of the permanent magnet synchronous motor (PMSM) is shown in Table 1:

The simulation parameters of the controller are listed as follows:

1) PI controller: $k_p = 15$, $k_i = 800$.

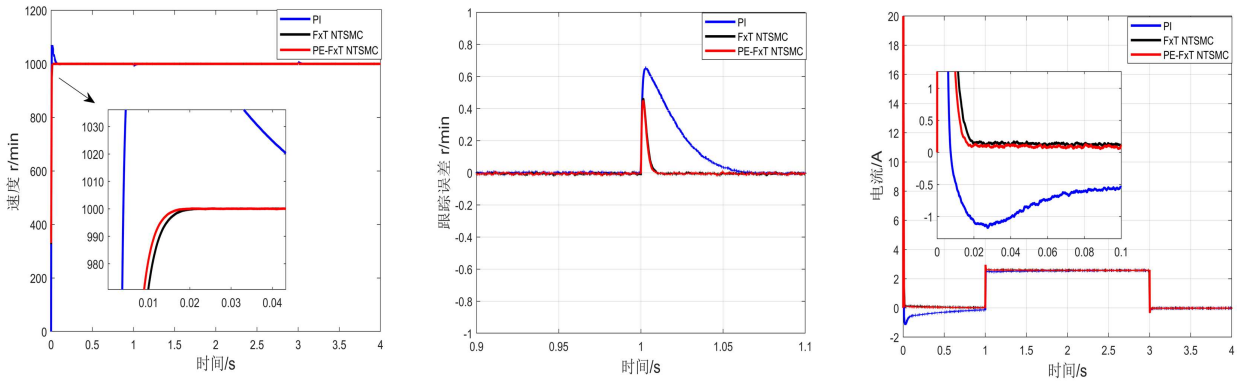

(a) Speed tracking (b) Tracking error (c) Control input

Figure 3. The response curve at the constant speed s_1.

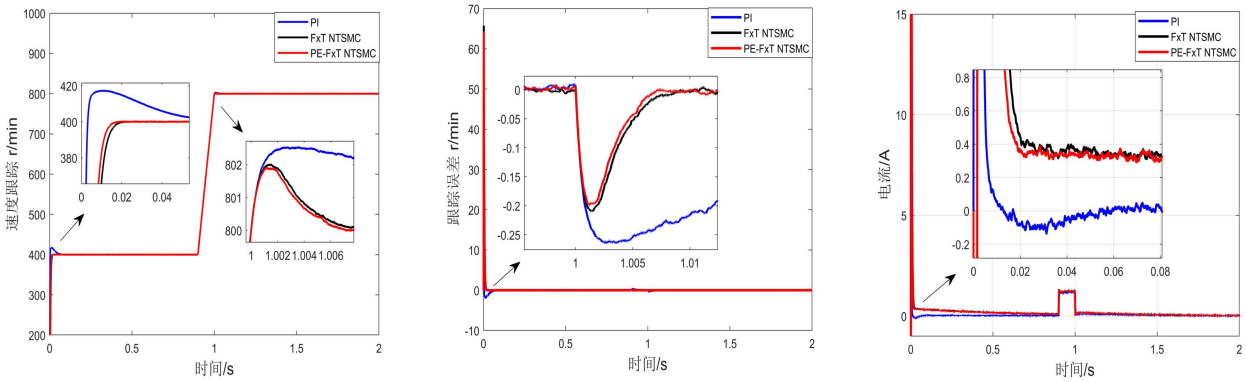

(a) Speed tracking (b) Tracking error (c) Control input

Figure 4. The response curve at the constant speed s_2.

Table 1. Parameters of the system.

Description	Value	Unit
Ψ_f	0.32	Wb
J	0.0027	$Kg{\cdot}m$
R	1.84	Ω
L	6.65	mH
P	1.5	kW
n_p	4	/

2) FxT-NTSMC: $k_1 = 300$, $k_2 = 320$, $c_1 = 25$, $c_2 = 50$, $a = 20$, $b = 62$, $\tau = 0.9$, $\nu_1 = 12$, $\nu_2 = 0.7$, $\varepsilon = 0.04$.

3) PE-FxT-NTSMC: $\Gamma = 20I$, $\kappa_1 = \kappa_2 = 10I$, $\gamma_1 = 0.5$, $\gamma_2 = 250$.

Figures 3(a), (b), and (c) respectively illustrate the simulation results of speed tracking performance, tracking error, and control input during startup at a target speed of $1000r/\min$ under the action of load torque T_L using different controllers. Figures 4(a), (b), and (c) present the corresponding results for the target speed s_2. The simulation results shown in Figure 3 and Figure 4 demonstrate that, compared with the conventional PI control and the FxT-NTSMC method, the proposed PE-FxT-NTSMC approach achieves faster response, stronger disturbance rejection, and more optimized control input.

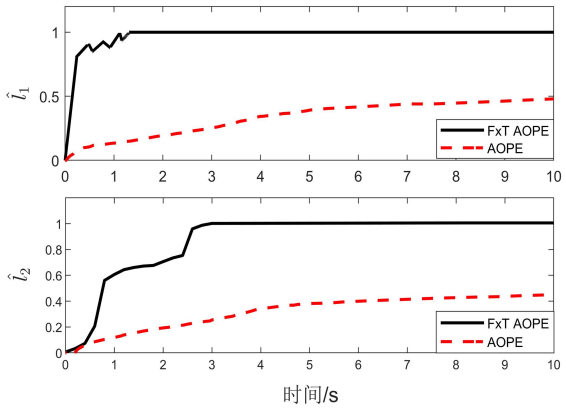

Figure 5. The estimation results of $\hat{l}_1$ and $\hat{l}_2$.

Figures 5 and 6 present the simulation results of parameters l_1, l_2, and D_1, D_2 under two parameter estimation methods: FxT-AOPE and AOPE. The simulation results indicate that the proposed fixed-time optimal adaptive law significantly accelerates the convergence of the estimated parameters to their true values, while maintaining high estimation accuracy. Experimental results further

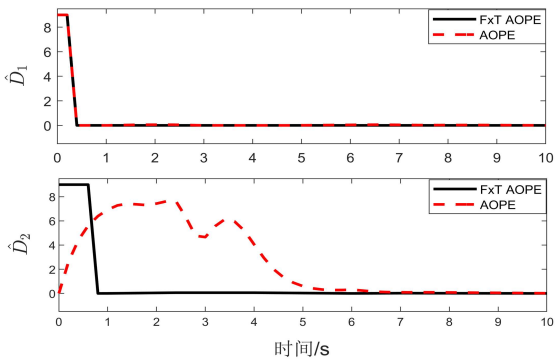

Figure 6. The estimation results of $\hat{D}_1$ and $\hat{D}_2$.

confirm that the fixed-time optimal adaptive law based on parameter estimation error effectively enhances the estimation speed and substantially improves the accuracy of estimation performance.

6.2 Experimental Verification

Experimental tests were carried out using the LINKS-RT real-time simulation platform to verify the effectiveness of the control algorithm proposed in this chapter. In the LINKS-RT platform, the inverter switching frequency was set to 10kHz, and the sampling period of the real-time simulator was set to $100us$. The experiments mainly evaluated the following aspects: the speed overshoot and startup time of the PMSM under different control strategies during startup; the speed fluctuation and recovery performance under external load variations; and the estimation accuracy of AOPE and FxT-AOPE. Through these experiments, the performance of the proposed control method was comprehensively assessed in terms of control accuracy, disturbance rejection capability, and parameter estimation precision. To ensure fairness in comparison, all experimental parameters were kept the same except for those specific to each controller. The experimental tests were carried out using the LINKS-RT real-time simulation platform, as shown in Figure 9.

1) PI: $k_p = 0.05$, $k_i = 0.5$.

2) FxT-NTSMC: $k_1 = 20$, $k_2 = 30$, $c_1 = c_2 = 5$, $a = 1.5$, $b = 2$, $\tau = 0.4$, $\nu_1 = 5$, $\nu_2 = 0.5$, $\varepsilon = 0.02$.

3) PE-FxT-NTSMC: $\Gamma = 0.3I$, $\mathrm{K}_1 = \mathrm{K}_2 = 5I$, $\gamma_1 = 0.1$, $\gamma_2 = 25$.

The corresponding experimental results are shown in Figures 7 to 13. Tables 2 and 3 present the performance metrics of the experiments, including Settling Time (ST), Overshoot (OS), Overall Speed Fluctuation (OSF), and Overall Recovery Time (ORT). Specifically, ORT and OSF are defined as: $ORT = t_1 + t_2$, $OSF = |\omega_1| + |\omega_2|$. where t_1 and t_2 represent the recovery times when the load torque suddenly increases or decreases, respectively, and ω_1 and ω_2 denote the corresponding peak deviations in rotational speed.

Experiment 1: Results of Constant Speed Experiment

As shown in Figure 7(a), compared to the PI controller and the traditional FxT-NTSMC control strategy, the PE-FxT-NTSMC control scheme exhibits almost zero overshoot during the initial phase of speed tracking. This indicates that the PE-FxT-NTSMC control strategy significantly improves the oscillation and overshoot issues in the speed tracking process, resulting in a smoother tracking curve during the speed regulation process.

Additionally, as shown in Figure 7(a), in terms of speed tracking, the PE-FxT-NTSMC control strategy outperforms both the PI controller and the traditional FxT-NTSMC control strategy. More specifically, the ST of the PE-FxT-NTSMC control strategy is 0.26s, which is the shortest among the three control methods. The traditional FxT-NTSMC control strategy has an ST of 0.45s, and the PI strategy has an ST of 0.58s. Therefore, the PE-FxT-NTSMC control strategy takes the least amount of time to converge to the desired speed.

Table 2. The performance index of Experiment 1.

Index	ST(s)	OS(%)	ORT(s)	OSF(rpm)
PE-FxT-NTSMC	0.26	0	0.28	72
FxT-NTSMC	0.45	0.5	0.31	62
PI	0.58	4.6	0.39	86

The results shown in Table 2 and Figures 7(a) and (b) indicate that under the PE-FxT-NTSMC scheme, the PMSM system recovers from the disturbance load impact within 0.14 seconds with minimal fluctuation (i.e., 36 rpm). By comparison, the PE-FxT-NTSMC scheme outperforms the traditional FxT-NTSMC control strategy and the PI method, effectively guiding the system state to approach the sliding mode surface more smoothly, achieving faster convergence speed, and significantly shortening the system's response time. The introduction of the parameter estimation strategy allows the unknown and varying parameters in the motor model to be updated in real-time. This enables the controller to dynamically adjust the control

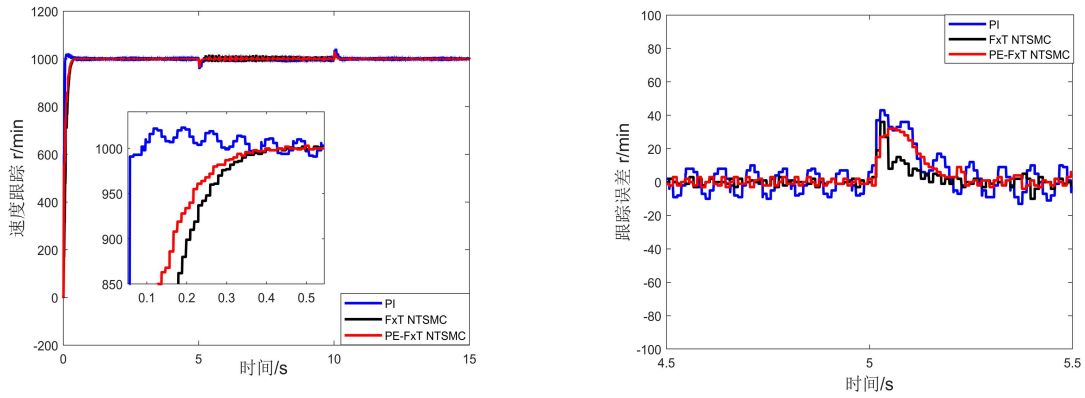

(a) Speed tracking (b) Tracking error

Figure 7. The response curve of Experiment 1.

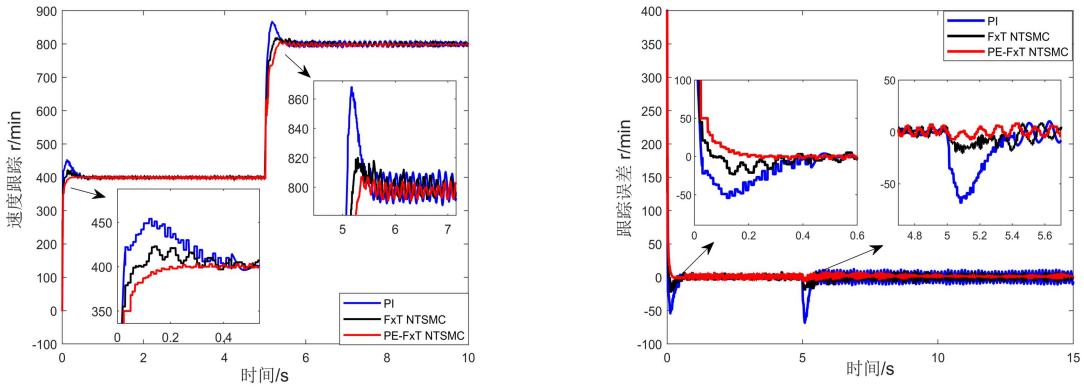

(a) Speed tracking (b) Tracking error

Figure 8. The response curve of Experiment 2.

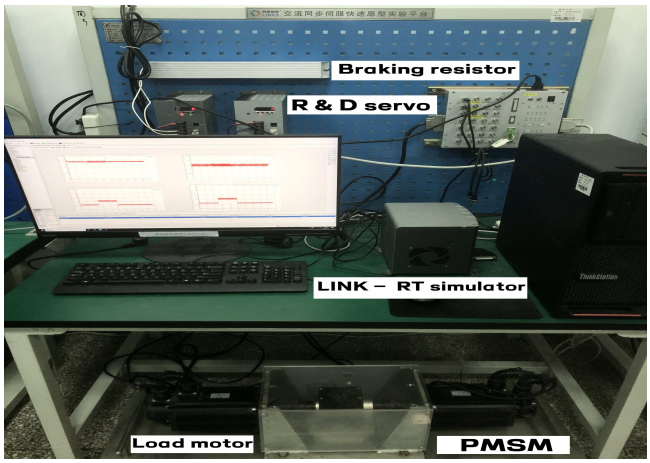

Figure 9. LINKS-RT Semi-Physical Simulation Experiment Platform.

strategy based on the updated motor parameters, thereby reducing the negative impact of parameter changes on system performance. This not only enhances the system's disturbance rejection capability but also improves its ability to track the desired signal quickly and accurately, further boosting the system's robustness and control precision.

Experiment 2: Results of Variable Speed Experiment

This experiment tests the system response at different speeds, where the motor starts at a speed of $400r/\min$ and adjusts to $800r/\min$ at 5 seconds. As shown in Figure 8, during the acceleration from low speed $400r/\min$ to high speed $800r/\min$, the overshoot of the PE-FxT-NTSMC scheme is nearly zero, much lower than that of the PI controller and the FxT-NTSMC strategy. Particularly during the acceleration phase, the PE-FxT-NTSMC controller maintains a low overshoot and steadily tracks the desired speed. In contrast, during the transient response phase, the PI controller exhibits significant dynamic overshoot and high-frequency oscillations, while the FxT-NTSMC strategy only shows slight dynamic overshoot and jitter. Once the speed stabilizes, the PE-FxT-NTSMC scheme demonstrates a smaller steady-state error and higher accuracy, especially in the stable state after speed regulation is completed, where the error is close to zero. Both the PI controller and FxT-NTSMC scheme show some steady-state errors, which affect the system's stability.

The results shown in Table 3 and Figures 8 (a) and (b) demonstrate that the PE-FxT-NTSMC control scheme exhibits exceptional system response time during

Table 3. The performance index of Experiment 2.

Index	ST(s) $400r/\min$	OS(%) $400r/\min$	ORT(s) $800r/\min$	OSF(rpm) $800r/\min$
PE-FxT-NTSMC	0.198	0	0.32	1.75
FxT-NTSMC	0.245	5.75	0.65	5
PI	0.322	13.5	0.68	8.5

the variable speed process, with a convergence time significantly shorter than that of the other two control strategies. More specifically, at speeds of $400r/\min$ and $800r/\min$, the ST of the PE-FxT-NTSMC control strategy is 0.198s and 0.32s, respectively, the lowest among the three control methods. The traditional FxT-NTSMC control strategy are 0.245s and 0.65s, while the PI strategy are 0.322s and 0.68s. Therefore, the PE-FxT-NTSMC control strategy takes the least amount of time to converge to the desired speed. Based on the variable speed experimental results, it is clear that the PE-FxT-NTSMC control scheme outperforms the PI controller and FxT-NTSMC strategy in terms of speed tracking accuracy, system response time, and robustness.

Experiment 3: Results of Parameter Estimation Experiment

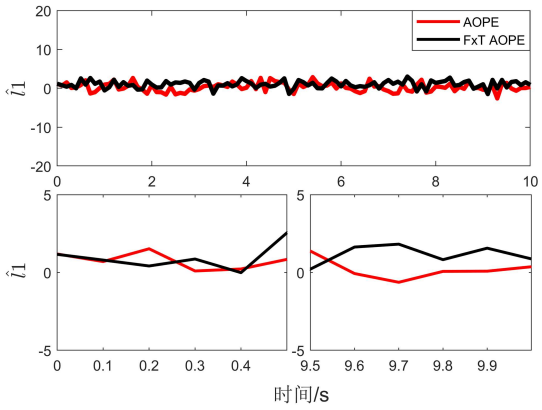

Figure 10. The estimation results of l_1.

Due to the ability of FxT-AOPE to quickly respond to changes in system parameters under fixed-time conditions, it ensures faster convergence speed and higher estimation accuracy. As shown in Figures 10 to 13, AOPE exhibits larger estimation errors and longer response times under the same operating conditions, whereas FxT-AOPE can rapidly track parameter changes in a very short time. This indicates that FxT-AOPE effectively reduces estimation errors when dealing with rapidly changing

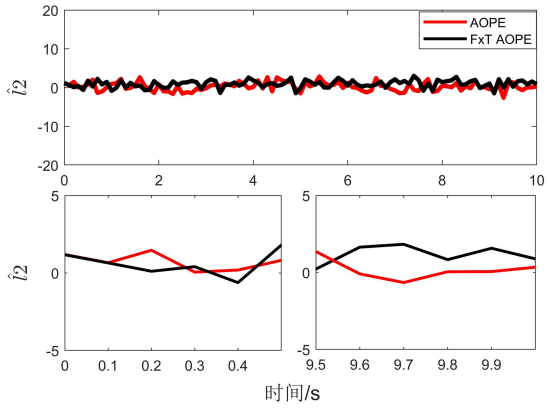

Figure 11. The estimation results of l_2.

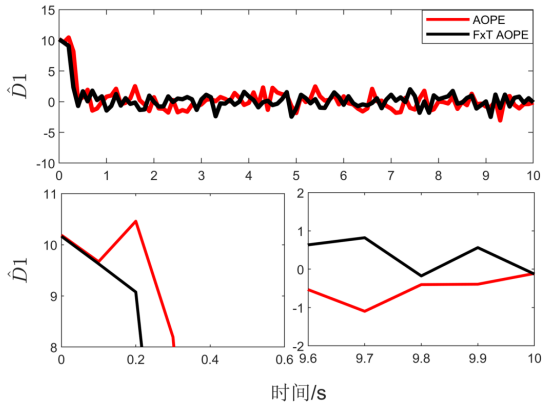

Figure 12. The estimation results of D_1.

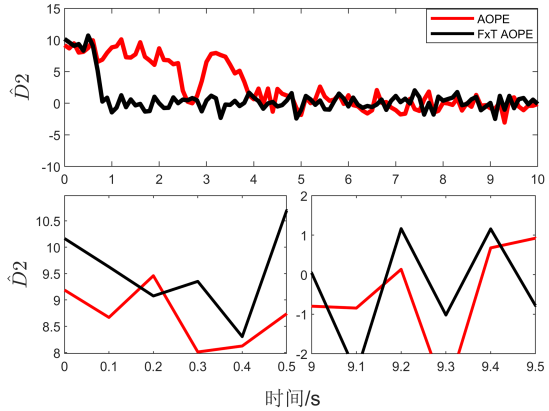

Figure 13. The estimation results of D_2.

system parameters, enhancing the adaptability to environmental changes of system. Compared to AOPE, FxT-AOPE not only achieves accurate estimation of unknown parameters in a shorter time, leading to faster parameter convergence, but also outperforms AOPE in estimation accuracy, maintaining high estimation precision under conditions of system parameter variations. Additionally, FxT-AOPE demonstrates stronger robustness when dealing with parameter fluctuations and faster transient response, which can significantly improve system performance. In practical control systems, using adaptive laws with time-varying gains and fixed-time conditions

can significantly enhance system robustness and estimation performance. The use of FxT-AOPE allows for better handling of unknown parameter changes and environmental disturbances, thereby improving the system's adaptability and control precision.

7 Conclusion

This chapter proposes a cost function based FxT AOPE method and its related control scheme for servo systems with asymmetric dead zone input nonlinearity. Firstly, design an approximate asymmetric dead zone for CPLNN, construct a cost function for estimation error, derive time-varying gain in adaptive law, and achieve AOPE. Then, the terminal sliding mode manifold was combined with the proposed learning algorithm to propose FxT-NTSMC, ensuring fixed time convergence of estimation error and tracking error simultaneously. The simulation and experimental results on the permanent magnet synchronous motor platform have verified the effectiveness of this method.

Data Availability Statement

Data will be made available on request.

Funding

This work was supported by the National Natural Science Foundation of China under Grant 62173194.

Conflicts of Interest

The authors declare no conflicts of interest.

Ethical Approval and Consent to Participate

Not applicable.

References

[1] Kashif, M., & Singh, B. (2021). Solar PV-fed reverse saliency spoke-type PMSM with hybrid ANF-based self-sensing for water pump system. *IEEE Journal of Emerging and Selected Topics in Power Electronics, 10*(4), 3927–3939. [CrossRef]

[2] Ping, Z., Jia, Y., Li, Y., Huang, Y., Wang, H., & Lu, J. G. (2022). Global position tracking control of PMSM servo system via internal model approach and experimental validations. *International Journal of Robust and Nonlinear Control, 32*(16), 9017-9033. [CrossRef]

[3] El Makrini, I., Rodriguez-Guerrero, C., Lefeber, D., & Vanderborght, B. (2016). The variable boundary layer sliding mode control: A safe and performant control for compliant joint manipulators. *IEEE Robotics and Automation Letters, 2*(1), 187-192. [CrossRef]

[4] Nie, L., Zhou, M., Cao, W., & Huang, X. (2023). Improved nonlinear extended observer based adaptive fuzzy output feedback control for a class of uncertain nonlinear systems with unknown input hysteresis. *IEEE Transactions on Fuzzy Systems, 31*(10), 3679-3689. [CrossRef]

[5] Nguyen, V. T., Bui, T. T., & Pham, H. Y. (2023). A finite-time adaptive fault tolerant control method for a robotic manipulator in task-space with dead zone, and actuator faults. *International Journal of Control, Automation and Systems, 21*(11), 3767-3776. [CrossRef]

[6] Zhang, Z., Yang, C., & Ge, S. S. (2022). Decentralized adaptive control of large-scale nonlinear systems with time-delay interconnections and asymmetric dead-zone input. *IEEE Transactions on Systems, Man, and Cybernetics: Systems, 53*(4), 2259-2270. [CrossRef]

[7] Ibrir, S., & Su, C. Y. (2010). Simultaneous state and dead-zone parameter estimation for a class of bounded-state nonlinear systems. *IEEE transactions on control systems technology, 19*(4), 911-919. [CrossRef]

[8] Na, J., He, H., Huang, Y., & Dong, R. (2021). Adaptive estimation of asymmetric dead-zone parameters for sandwich systems. *IEEE Transactions on Control Systems Technology, 30*(3), 1336-1344. [CrossRef]

[9] Na, J., Xing, Y., & Costa-Castelló, R. (2018). Adaptive estimation of time-varying parameters with application to roto-magnet plant. *IEEE Transactions on Systems, Man, and Cybernetics: Systems, 51*(2), 731-741. [CrossRef]

[10] He, H., Na, J., Wu, J., Huang, Y., & Xing, Y. (2023). Fixed-time adaptive parameter estimation for Hammerstein systems subject to dead-zone. *IEEE Transactions on Industrial Electronics, 71*(4), 3862-3872. [CrossRef]

[11] Chiu, S. (2012). Derivative and integral terminal sliding mode control for a class of MIMO nonlinear systems. *Automatica, 48*(2), 316–326. [CrossRef]

[12] Huang, Y., & Jia, Y. (2018). Adaptive fixed-time six-DOF tracking control for noncooperative spacecraft fly-around mission. *IEEE Transactions on Control Systems Technology, 27*(4), 1796-1804. [CrossRef]

[13] Zhang, Y., Tang, S., & Guo, J. (2018). Adaptive terminal angle constraint interception against maneuvering targets with fast fixed-time convergence. *International Journal of Robust and Nonlinear Control, 28*(8), 2996-3014. [CrossRef]

[14] Ni, J., Liu, L., Liu, C., Hu, X., & Li, S. (2016). Fast fixed-time nonsingular terminal sliding mode control and its application to chaos suppression in power system. *IEEE Transactions on Circuits and Systems II: Express Briefs, 64*(2), 151-155. [CrossRef]

[15] Utkin, V., Poznyak, A., Orlov, Y., & Polyakov, A. (2020). Conventional and high order sliding mode control. *Journal of the Franklin Institute, 357*(15), 10244-10261. [CrossRef]

[16] Na, J., Chen, A. S., Herrmann, G., Burke, R., & Brace, C. (2017). Vehicle engine torque estimation via unknown input observer and adaptive parameter estimation. *IEEE Transactions on Vehicular Technology, 67*(1), 409-422. [CrossRef]

[17] Wang, S. (2004). General constructive representations for continuous piecewise-linear functions. *IEEE Transactions on Circuits and Systems I: Regular Papers, 51*(9), 1889-1896. [CrossRef]

[18] Cui, L., Jin, N., Chang, S., Zuo, Z., & Zhao, Z. (2022). Fixed-time ESO based fixed-time integral terminal sliding mode controller design for a missile. *ISA transactions, 125*, 237-251. [CrossRef]

[19] Liu, C., & Liu, Y. (2022). Finite-time stabilization with arbitrarily prescribed settling-time for uncertain nonlinear systems. *Systems & Control Letters, 159*, 105088. [CrossRef]

[20] Chen, C., Li, L., Peng, H., Yang, Y., Mi, L., & Wang, L. (2019). A new fixed-time stability theorem and its application to the synchronization control of memristive neural networks. *Neurocomputing, 349*, 290-300. [CrossRef]

[21] Ioannou, P. A., & Sun, J. (2012). *Robust adaptive control*. Courier Corporation.

[22] Ioannou, P. A., & Sun, J. (1996). *Robust adaptive control* (Vol. 1, pp. 75-76). Upper Saddle River, NJ: PTR Prentice-Hall.

[23] Na, J., Mahyuddin, M. N., Herrmann, G., Ren, X., & Barber, P. (2015). Robust adaptive finite-time parameter estimation and control for robotic systems. *International Journal of Robust and Nonlinear Control, 25*(16), 3045-3071. [CrossRef]

Shubo Wang received the Ph.D. degree in control science and engineering from the Beijing Institute of Technology, Beijing, China, in 2017. He is currently a professor at the School of Automation, Kunming University of Science and Technology. He has coauthored one monograph and more than 70 international journal and conference papers. His current research interests include adaptive control, parameter estimation, neural network, servo system, robotic, nonlinear control and applications for robotics and motor driving systems.

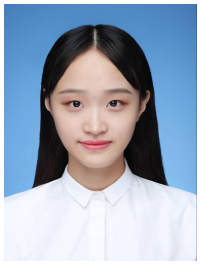

Xue Wang received the B.S. degree in electrical engineering and automation from Shandong Agricultural University, Taian, China, in 2022. She is currently working toward the M.S. degree in the control science and engineering, Qingdao University, Qingdao, China. Her current research interests include the dead zone compensation and tracking control of permanent magnet synchronous motor.